Published in final edited form as:
Magn Reson Med. 2006 January ; 55(1): 16–22. doi:10.1002/mrm.20742.

Combination of 2D Sensitivity Encoding and 2D Partial Fourier Techniques for Improved Acceleration in 3D Contrast-Enhanced MR Angiography

Houchun H. Hu, **Ananth J. Madhuranthakam**, **David G. Kruger**, **James F. Glockner**, and **Stephen J. Riederer***
Magnetic Resonance Imaging Laboratory, Department of Radiology, Mayo Clinic College of Medicine, Rochester, Minnesota, USA

Abstract

Sensitivity encoding (SENSE) and partial Fourier (PF) techniques both reduce MRI acquisition time. Two-dimensional SENSE uses coil sensitivities to unfold aliasing in the phase/ slice-encoding plane. One-dimensional PF and homodyne reconstruction are routinely applied in the frequency/phase-encoding plane to compensate for nonsampled *k*-space of the presumed real magnetization. Recently, a modified 3D elliptical centric acquisition was proposed to facilitate 2D-PF and homodyne reconstruction on an undersampled phase/slice-encoding plane. In this work we hypothesized that this 2D-PF technique can be combined with 2D-SENSE to achieve a greater acceleration factor than what each method can provide separately. Reconstruction of data whereby SENSE and PF are applied along the same axes is described. Contrast-enhanced MR angiography (CE-MRA) results from experiments using four receiver coils in phantom and volunteer studies are shown. In 11 volunteer studies, the SENSE-PF-homodyne technique using sevenfold acceleration (4× SENSE, 1.7× PF) consistently provided high-diagnostic-quality images with near 1-mm isotropic resolution in acquisition times of <20 s.

Keywords

2D-SENSE; 2D-partial Fourier; 2D-homodyne; fast MRI; contrast-enhanced MR angiography

Three-dimensional (3D) contrast-enhanced MR angiography (CE-MRA) has become a well accepted technique for clinical imaging of many vascular regions (1,2). Since it was first described over a decade ago (3,4), a number of methods have been developed to improve the attainable spatial resolution. These include shorter repetition times (TRs), faster and stronger encoding gradients, and specific *k*-space acquisition techniques. One example of the latter is the elliptical centric (EC) view order (5,6), which because of its intrinsic suppression of venous signal allows extensive acquisition times and potentially high spatial resolution. Another example is projection reconstruction (PR) (7,8), which provides high spatial resolution with robust insensitivity to undersampling artifacts. These methods continue to evolve.

Simultaneously with these advances in CE-MRA has been the development of parallel imaging methods (9–11), in which sparse sampling is implemented along the phase-encoding axes. These have been successfully applied in various ways to CE-MRA, resulting in reduced scan time, improved spatiotemporal resolution, and additional venous suppression (12–17). Partial

*Correspondence to: Stephen J. Riederer, Ph.D., Magnetic Resonance Laboratory, Mayo Clinic College of Medicine, 200 1st Street S.W., Rochester, MN 55905. E-mail: riederer@mayo.edu.

Fourier (PF) imaging is an additional, older method for accelerating data acquisition (18,19). Under the assumption that the magnetization of the imaging object is purely real, the resultant conjugate symmetric property of *k*-space is exploited, allowing in principle a twofold reduction in the number of measured data points. In practice, the actual time savings is less than twofold, due to the need to collect additional samples near central *k*-space to account for a phase map across the imaging plane. Current PF techniques are typically implemented in one dimension, either along the frequency readout axis (partial echo) or the phase-encoding axis (partial number of excitations (NEX)). Even with these advances there continues to be a need for improved spatial resolution (near 1 mm isotropic) and shorter acquisition times in areas such as MRA of the intracranial and the extended peripheral vasculature. Such spatial-resolution demands can be challenging, since they inherently lead to long scan times, and are complicated by the limited temporal window between arterial and adjacent venous contrast enhancement, especially in patients with certain vascular diseases.

Recently, a modified 3D EC view-order technique was introduced to improve spatial resolution in a given scan time in CE-MRA. The technique extends PF to two dimensions in a sparsely sampled phase/slice-encoding plane, and applies subsequent 2D homodyne detection to reconstruct nonacquired *k*-space views (20,21). The goal of this work was to describe the integration of 2D-SENSE (22,23) with this modified EC sampling scheme. We hypothesized that the individual acceleration factors of 2D-SENSE and 2D-PF could be synergistically combined into a single 3D acquisition (hereafter referred to as SENSE-PF) to obtain a higher net acceleration factor than could be achieved by each method separately. The proposed SENSE-PF method should be distinguished from acquisitions using 2D-SENSE and a partial echo readout, where the SENSE-encoded axes (phase/slice) are independent of the PF axis (frequency). In contrast, the present work addresses the unique case in which both 2D-SENSE and 2D-PF operate on the same set of phase- and slice-encoding axes.

Using a four-element receiver array, we found that the maximum 2D-SENSE factor of 4 ($R_Y = R_Z = 2$) could be robustly achieved, while an additional speed-up of 1.7 was obtained with PF, yielding a net sevenfold acceleration compared to corresponding nonaccelerated fully-sampled cases. We first briefly review the hybrid EC-PR *k*-space sampling pattern in the phase/slice-encoding plane, and describe the resultant combination with 2D-SENSE. The reconstruction algorithm for the SENSE-PF data is then described. The technique was tested experimentally with a phantom and in CE-MRA studies of the lower legs in 14 human volunteers. We show that the results obtained with 2D-SENSE (4×) and SENSE-PF (7×) exhibit comparable near 1-mm isotropic spatial resolution. In all experiments, 2D-SENSE was used to improve lateral (*Y*) and slice (*Z*) spatial resolution, while PF undersampling afforded a further 1.7× reduction in scan time, the latter being equivalent in speed-up to a 58% partial NEX acquisition.

Materials and Methods

Hybrid EC-PR and 2D-PF

Figure 1a schematically shows the previously described undersampled EC technique (20,21) in the k_Y-k_Z plane, modified from a standard 3D Cartesian EC acquisition. The figure superimposes that method's *k*-space sampling footprint (gray areas) on top of a fully sampled k_Y-k_Z grid. Frequency encoding is perpendicular to the page, with each black dot representing an individual phase-encoded echo. For clarity, a reduced number of view positions are shown than are actually acquired. During data sampling, only views that fall within the footprint are collected, which constitutes approximately 58% (PF reduction factor, $R_{PF} = 1.7$) of the entire rectangular k_Y-k_Z grid. The sampling footprint utilizes 2D-PF along both the k_Y and k_Z phase-encoded axes. Thus for this 3D EC-PR technique, a full echo along the frequency readout is required. The EC-PR footprint contains several traits that facilitate 2D homodyne processing.

First, a fully-sampled central ellipse containing approximately 20% of all acquired views is used to accurately form the homodyne phase map (19). Second, multiple radial sectors, or "vanes," extending from the ellipse make up an outer undersampled annulus. As the acquisition proceeds, all views are acquired in the conventional EC time-order, starting with the central ellipse. This is followed by selective sampling of the outer annulus where views are asymmetrically sampled (dotted lines) across the k_Y-k_Z plane. Thus a sampled ($+k_Y$, $+k_Z$) view in the annulus does not have a sampled conjugate ($-k_Y$, $-k_Z$). Asymmetric sampling is specifically implemented to allow the subsequent 2D homodyne process to account for the nonsampled views by using the phase information obtained from the central ellipse (18,19, 24). PF and homodyne reconstruction are not possible if symmetrical vanes are adopted. Since both $k_{Y\text{-}max}$ and $k_{Z\text{-}max}$ frequencies acquired by the modified technique are the same as those of a corresponding fully sampled case, the spatial resolutions along *Y* and *Z* should be comparable.

Integration With 2D-SENSE

Figure 1b illustrates the extension of the aforementioned sampling pattern to 2D-SENSE. The k_Y-k_Z axes labels now represent that of a fourfold SENSE-encoded acquisition with R_{SENSE} = 2 along each of the two phase-encoding directions. This is reflected by the twofold increase in sampling intervals Δk_Y and Δk_Z in comparison to Fig. 1a. The number of echoes in the k_Y-k_Z grid has been reduced by four. Simple Fourier reconstruction of Fig. 1b leads to an image that is twice-aliased in both the *Y* and *Z* directions.

SENSE-PF Image Reconstruction

All *k*-space sampling was performed on a Cartesian grid, and hence image reconstruction was achieved by standard Fourier transformation. Previous work (25) addressed the algorithmic steps needed to reconstruct 1D SENSE-PF data in 2D MRI where SENSE and homodyne reconstruction are performed along the phase-encoding axis in the k_X-k_Y plane. In Fig. 2, extension of the reconstruction algorithm to the proposed 2D-SENSE-PF technique in the k_Y-k_Z plane is described. Both the SENSE unaliasing (10) and the homodyne detection (18,19) steps of the algorithm are based on previously described methods. However, the order in which these two processes are performed is critical. Specifically, SENSE unfolding must be performed prior to homodyne phase correction because the latter removes phase information from the aliased data set that is crucial to the SENSE unaliasing process.

As shown in Fig. 2, raw data from *N* coils are first Fourier transformed along the readout (*X*) axis (step I). Data from each coil are then directed along two paths: one representing a low-pass filtered image in which only views sampled within the central ellipse are reconstructed, and one representing a high-pass filtered image in which all sampled views are used, but with unity weighting for those located in the ellipse and factor 2 weighting for those asymmetrically sampled in the outer annulus (step II). The two resulting sets of *N* low-pass filtered images and *N* high-pass filtered images are then separately unfolded with standard SENSE processing, yielding a single low-pass image and a single high-pass image, each of which is deterministically unaliased (step III). The final image is created by taking the real part of the high-pass filtered reconstruction after it is corrected for phase using information obtained from the low-pass reconstruction (step IV).

In addition to 2D homodyne reconstruction of the nonsampled k_Y-k_Z views, a simpler, sparse reconstruction can be performed in which nonsampled measurements are zero-filled. This option does not require homodyne detection or phase correction and therefore the raw data can directly undergo standard 2D-SENSE processing without having to be directed into two separate paths.

Coil Configuration

The receiver coil array used in this work consisted of four elements grouped into two pairs. For all experiments, coil placement involved two elements (one pair) positioned anterior and two elements positioned posterior to the imaging object. In the volunteer examinations, the elements were strapped securely about the subject's lower legs. Each element measured 40 cm (superior/inferior (S/I)) × 15 cm (right/left (R/L)) and exhibited distinct sensitivities to the anterior and posterior sections of each leg. The coil configuration was chosen for ease of setup and patient comfort. According to Ref. 10, a maximum SENSE acceleration factor equaling the total number of receivers is possible to achieve. In this work, a maximum speed-up of 4 was achieved by distributing R_Y and R_Z across the two phase-encoding axes in several ways. Geometry factors (*g*-factors) were calculated (10) using profiles measured from the coils used in this work of two cylindrical homogeneous agar phantoms (15 cm diameter) that simulated the two lower legs imaged in the in vivo studies. Favorable *g*-values in the range of 1–2 were obtained for the 2D-SENSE ($R_Y = 2$, $R_Z = 2$) scenario implemented in this work, which were far superior to *g*-values (>10) obtained when the same $R = 4$ acceleration was applied solely in either the *Y* or *Z* direction. This preference for implementing 2D-SENSE over 1D SENSE to achieve the same net acceleration is consistent with previous studies (22,23).

SENSE Coil Calibration

SENSE reconstruction requires a priori calibration of coils to obtain accurate maps of their sensitivity profiles within the imaging volume (10). For the present work we adopted a calibration protocol whereby profiles of individual coils are obtained by normalization with a sum-of-squares combination. The resolution of the calibration images is twofold coarser than that of the SENSE-acquisition along the SENSE-encoded directions (*Y*-R/L, *Z*-anterior/posterior (A/P)). A gradient-echo pulse sequence with repetition/ echo time (TR/TE) = 15/3 ms, flip angle = 10°, NEX = 1, and bandwidth (BW) = ±31.26 kHz was used.

Phantom Experiments

All experiments, both phantom and in vivo, were performed on a 1.5T Signa LX scanner (GE Medical Systems, Milwaukee, WI, USA) with a four-coil array. Data reconstruction was performed offline with SENSE-PF data sets following the algorithm described in Fig. 2. The SENSE-PF sampling scheme was tested on a resolution phantom using a 3D gradient-echo sequence. Resolution bars were placed within the axial *Y*-*Z* plane. First, a fully-sampled reference scan using FOV = 24 cm, a 256 (X-read) × 128 (Y-phase) × 44 (*Z*-slice) sampling matrix, 4.8 mm coronal partitions, flip angle = 30°, NEX = 1, BW = ±31.26 kHz, full echo, and TR/TE = 20/3 ms was obtained, which required 1 min 55 s of scan time. This was then followed by a fully sampled fourfold SENSE acquisition with ($R_Y = R_Z = 2$) using the same sampling matrix, which improved phase and slice resolution each by twofold while maintaining the 1 min 55 s scan time. Third, the SENSE-PF acquisition was implemented. Only 58% of the views in the SENSE scan were acquired, which reduced the scan time to 66 s. A fully sampled nonaccelerated acquisition that equaled the spatial resolution of the fourfold SENSE scan would have taken 7 min 40 s using the same acquisition parameters. The SENSE-PF scan time thus represents a net sevenfold acceleration.

Volunteer CE-MRA Studies

CE-MRA examinations of the lower legs were approved by the institutional review board, and the SENSE-PF method was applied to 14 consecutive volunteers after they provided informed consent. For each examination, three contrast injections were given using an electronic injector (Medrad Spectris Solaris; Medrad, Inc., Indianola, PA, USA). The first, with 2 ml of gadolinium contrast (Omniscan; Nycomed Inc., Princeton, NJ, USA) at 3 ml/s and 15 ml of saline flush at 2 ml/s, determined the contrast arrival time at the popliteal trifurcation and the

subsequent acquisition trigger time of the larger contrast dose. This was followed by both a standard EC view-order 2D-SENSE-only scan with maximum fourfold acceleration, and the proposed SENSE-PF scan with sevenfold net acceleration. The order of the two scans was randomized. For each acquisition, 19 ml of contrast at 3 ml/s and 15 ml of saline at 2 ml/s were injected. The two scans were separated by a minimum 10-min waiting period to allow contrast from the first injection to adequately clear the vascular system. A corresponding mask data set was also acquired prior to each contrast dose and used for subsequent image subtraction. For these in vivo studies, SENSE was applied to improve spatial resolution (R_{SENSE} = 4), while PF was used to shorten the scan time (R_{PF} = 1.7). A 3D spoiled gradient-echo sequence was used in a coronal format with the following parameters: FOV_X = 40 cm, FOV_Y = 28–30 cm, a 256 (*X*-read) × 128 (*Y*-phase) × 44-48 (*Z*-slice) sampling matrix, 1.0–1.5 mm partitions, flip angle = 30°, BW = ±62.5 kHz, full echo, NEX = 1, and TR/TE = 6/3 ms. The *Y-Z* encoding was applied along the (R/L) × (A/P) directions, and the volume of excitation encompassed the full extent of the anatomy along these two dimensions. The 2D-SENSE acquisition typically took 34–37 s to complete, whereas the SENSE-PF acquisition took 19–20 s. For comparison purposes, a fully phase-encoded 2D-SENSE acquisition with a partial echo along the frequency readout axis would have taken 29 s. Thus, 2D-SENSE with PF along the readout axis represents only a 1.2× speed-up, since 62.5% (160/256) of the echo is acquired and consequently reduces TR by only 0.8 ms.

Evaluation of CE-MRA Studies

Coronal and sagittal maximum intensity projections (MIPs) of the 2D-SENSE and SENSE-PF reconstructions were collectively reviewed by the authors. For each of the 11 cases, 2D-SENSE and SENSE-PF images were individually scored under two categories. The first was based on a five-point scale reflecting each reconstruction's overall diagnostic quality (0 = nondiagnostic, 1 = marginally adequate, 2 = moderately acceptable, 3 = good, and 4 = excellent). Incorporated into this scoring were considerations of the signal-to-noise ratio (SNR), spatial resolution, and lack of reconstruction artifacts. The second category was a three-point scale reflecting the visibility of secondary arterial vessels originating from the popliteal, peroneal, anterior tibial, or posterior tibial arteries (0 = secondary vessels not visualized, 1 = marginally visualized, and 2 = well visualized). The scores were reached by consensus.

Results

Figure 3 illustrates reconstructed results from the phantom study, with axial reformatted images depicting the resolution bars in the *Y-Z* plane. In Fig. 3a the reference nonaccelerated, fully sampled image is shown, and it is evident that the resolution bars in rows 3 and 4 are not well resolved. In Fig. 3b the 4× SENSE-only reconstructed result is shown, with clear improvement in both phase and slice resolution, as demonstrated by row 3. Figure 3c and d show the sparse and homodyne reconstructions of the 7× SENSE-PF acquisition, respectively. Note that while the sparse reconstruction in Fig. 3c loses some resolution in comparison (arrow) to the SENSE-only result in Fig. 3b, due to zero-filling of nonsampled *k*-space, the homodyne reconstruction in Fig. 3d is able to comparably resolve the resolution bar set (2.38 line pairs/cm) in question. Both undersampled SENSE reconstructions demonstrate significant resolution improvement over the reference scan in Fig. 3a. The streaking artifacts in Fig. 3c and d are consistent with the PR-like sampling pattern of Fig. 1, and are restricted to the *Y-Z* axial plane.

High-quality 3D CE-MRA results were obtained with both the 2D-SENSE and the 2D-SENSE-PF methods in 11 out of 14 volunteer studies (the evaluation scores are summarized in Table 1). Comparisons were not available for three studies due to MR scanner equipment failure, misregistration artifact, and operator error. In all cases the three major vessels distal to the popliteal trifurcation were well visualized. Figure 4 shows representative images from two

studies. In Fig. 4a–d the acquired spatial resolution was 1.5 × 1.1 × 1.4 mm^3, with the 4× SENSE-only (a and c) and 7× SENSE-PF (b and d) acquisitions taking 34 and 19 s, respectively. For this volunteer (volunteer 3), the SENSE-PF acquisition was done using the first 19-ml contrast injection. In Fig. 4a and b coronal MIPs of the two scans are shown, and in Fig. 4c and d sagittal MIPs of the right leg are shown. Figure 4e–h illustrate similar image sets from volunteer 11, with an acquired voxel size of 1.5 × 1.2 × 1.3 mm^3. In all cases the popliteal, peroneal, and tibial arteries are comparably visualized and well resolved in the SENSE-only vs. SENSE-PF results. Furthermore, no venous overlay is present. Both lateral and slice resolution of SENSE and corresponding SENSE-PF images are comparable. Some minor loss in SNR and higher background signal are observed throughout the SENSE-PF vs. SENSE-only reconstructions, but at an insufficient level to adversely affect diagnostic quality. SENSE-related reconstruction artifacts are negligible and do not affect any vasculature in the images. The overall SNR in both the 2D-SENSE and SENSE-PF reconstructed results is more than adequate for diagnosis at the acquired spatial resolution.

Table 1 shows that all 2D-SENSE and SENSE-PF reconstructions received either good or excellent diagnostic-quality ratings. Multiple secondary arterial branches were well visualized in the majority of cases. The geniculate arteries, which supply blood to the knees, were seen bilaterally in all 22 image sets. In choosing either the 2D-SENSE or SENSE-PF reconstruction as the preferred image set for diagnosis, one of the authors (J.F.G.), an experienced MR radiologist, showed a marginal preference for the 2D-SENSE result in seven cases, no preference in two cases (volunteers 7 and 11), and slight preference for the SENSE-PF result in two cases (volunteers 3 and 5), based mainly on subtle differences in SNR and vessel conspicuity. However, the favored image set appears to be correlated to the technique that was implemented during the first of the two contrast injections, and the overall preference toward 2D-SENSE is likely not significant in this limited trial.

Discussion

In 2D-SENSE CE-MRA of the lower legs using four coil receivers, a maximum of fourfold acceleration can be achieved. In our experience, robust high-diagnostic-quality 3D angiograms with near 1-mm isotropic resolution have been consistently obtained with 2D-SENSE ($R_Y = R_Z = 2$) in approximately 35-s acquisitions. Furthermore, by combining 2D-SENSE with 2D-PF imaging with homodyne reconstruction, a net sevenfold acceleration was achieved, further reducing the scan time to less than 20 s. In comparison with 4× 2D-SENSE, the 7× SENSE-PF technique yields nearly equivalent spatial resolution and image quality. In addition, the shortened scan time further reduces the risk of venous overlay, and may be beneficial for patients with certain types of peripheral vascular disease (e.g., ischemic limbs, ulcers, and inflammation) that exhibits rapid venous return.

In this work the FOVs along the two SENSE-encoded directions encompassed the entire axial cross section of the lower legs. Specifically, the excitation slab included the full A/P extent of the legs (ca. 9–14 cm). Thus, if the method described here had been compared with a typical non-SENSE acquisition in which the excited slab was limited to only the principal peripheral arteries (ca. 7–10 cm of A/P coverage), the actual SENSE-acceleration would not have been as high. The issue of how to accurately perform 2D-SENSE imaging along a selected slab remains an ongoing area of research (22,23,26).

We expect that both the 2D-SENSE and the combined 2D-SENSE-PF techniques presented here are directly compatible with time-resolved imaging, by simple resampling of the previously sampled views, alternating the collection of vanes, or using view sharing (27–29). The principal assumption is that the a priori calculated coil sensitivity profiles for SENSE, and the overall phase maps used for homodyne reconstruction do not change over the time course

of the dynamic process being imaged. The first of these assumptions has been used in 1D-SENSE time-resolved imaging (12,14). While the present work targeted SENSE-PF application in CE-MRA, the proposed method can be expanded into other areas of 3D MRI, such as colonography, cholangio pancreatography, and whole-brain imaging, where high spatial resolution is desired within a limited acquisition time window.

Both SENSE and PF techniques are susceptible to intrinsic SNR loss because of either smaller voxel sizes or a reduction in the number of acquired *k*-space samples. Furthermore, for SENSE the expected SNR loss relative to a reference nonaccelerated acquisition depends on the SENSE acceleration and coil geometry factors (10). Similarly, the SNR of an image reconstructed from PF data is proportional to the square root of the number of acquired *k*-space data points, and is limited by the homodyne detection process. Nonetheless, as demonstrated by the high scores in Table 1, limited SNR was not an issue in any of the in vivo studies.

In developing the SENSE-PF method, we chose to maintain spatial resolution and reduce the number of acquired phase encodes. An alternative approach would have been to maintain the total number of sampled views of a standard 2D-SENSE acquisition, and hence the same scan time, but extend the vanes in the outer annulus farther into the k_Y-k_Z periphery. In effect, this option would increase the maximally sampled k_Y and k_Z spatial frequencies for additional spatial resolution improvement (20,21). Although a voxel size of 1 mm^3 may be adequate for visualizing the peripheral vasculature, this alternative SENSE-PF approach may be advantageous in neurovascular and breast CE-MRA, where submillimeter resolution may be desirable for visualizing small vascular beds.

Conclusions

The integration of 2D-SENSE and 2D-PF in the phase-encoding plane to accelerate 3D acquisitions by a factor as large as seven was demonstrated with the use of a four-element coil array and a modified EC-PR acquisition at the 1.5T field. The technique is robust in reconstruction and routinely yields diagnostic-quality and artifact-free images in fast, high-resolution 3D CE-MRA of the peripheral vasculature.

Acknowledgments

The authors thank Kelly T. Dunagan for coordinating the volunteer studies.

Grant sponsor: NIH; Grant numbers: HL70620; EB00212; EB004281.

References

1. Prince, MR.; Grist, TM.; Debatin, JF. 3D contrast MR angiography. Vol. 3rd. Berlin: Springer; 2003.
2. Schneider, G.; Prince, MR.; Meaney, JFM.; Ho, VB., editors. Magnetic resonance angiography. Milan: Springer; 2005.
3. Prince MR, Yucel EK, Kaufman JA, Harrison DC, Geller SC. Dynamic gadolinium-enhanced three-dimensional abdominal MR arteriography. J Magn Reson Imaging 1993;3:877–881. [PubMed: 8280977]
4. Prince MR. Gadolinium-enhanced MR angiography. Radiology 1994;191:155–164. [PubMed: 8134563]
5. Wilman AH, Riederer SJ. Improved centric phase encoding orders for three-dimensional magnetization-prepared MR angiography. Magn Reson Med 1996;36:384–392. [PubMed: 8875408]
6. Wilman AH, Riederer SJ, King BF, Debbins JP, Rossman PJ, Ehman RL. Fluoroscopically triggered contrast-enhanced three-dimensional MR angiography with elliptical centric view order: application to the renal arteries. Radiology 1997;205:137–146. [PubMed: 9314975]

7. Peters DC, Korosec FR, Grist TM, Block WF, Holden JE, Vigen KK, Mistretta CA. Undersampled projection reconstruction applied to MR angiography. Magn Reson Med 2000;43:91–101. [PubMed: 10642735]
8. Vigen KK, Peters DC, Grist TM, Block WF, Mistretta CA. Undersampled projection reconstruction imaging for time-resolved contrast-enhanced imaging. Magn Reson Med 2000;43:170–176. [PubMed: 10680679]
9. Sodickson DK, Manning WJ. Simultaneous acquisition of spatial harmonics (SMASH): fast imaging with radiofrequency coil arrays. Magn Reson Med 1997;38:591–603. [PubMed: 9324327]
10. Pruessmann KP, Weiger M, Scheidegger MB, Boesiger P. SENSE: sensitivity encoding for fast MRI. Magn Reson Med 1999;42:952–962. [PubMed: 10542355]
11. Griswold MA, Jakob PM, Heidemann RM, Nittka M, Jellus V, Wang J, Kiefer B, Haase A. Generalized autocalibrating partially parallel acquisitions (GRAPPA). Magn Reson Med 2002;47:1202–1210. [PubMed: 12111967]
12. Golay X, Brown SJ, Itoh R, Melhem ER. Time-resolved contrast-enhanced carotid MR angiography using sensitivity encoding (SENSE). AJNR Am J Neuroradiol 2001;22:1615–1619. [PubMed: 11559518]
13. Maki JH, Wilson GJ, Eubank WB, Hoogeveen RM. Utilizing SENSE to achieve lower station sub-millimeter isotropic resolution and minimal venous enhancement in peripheral MR angiography. J Magn Reson Imaging 2002;15:484–491. [PubMed: 11948840]
14. Muthupillai R, Vick GW 3rd, Flamm SD, Chung T. Time-resolved contrast-enhanced magnetic resonance angiography in pediatric patients using sensitivity encoding. J Magn Reson Imaging 2003;17:559–564. [PubMed: 12720265]
15. van den Brink JS, Watanabe Y, Kuhl CK, Chung T, Muthupillai R, Van Cauteren M, Yamada K, Dymarkowski S, Bogaert J, Maki JH, Matos C, Casselman JW, Hoogeveen RM. Implications of SENSE MR in routine clinical practice. Eur J Radiol 2003;46:3–27. [PubMed: 12648798]
16. Wilson GJ, Hoogeveen RM, Willinek WA, Muthupillai R, Maki JH. Parallel imaging in MR angiography. Top Magn Reson Imaging 2004;15:169–185. [PubMed: 15479999]
17. Hu HH, Madhuranthakam AJ, Kruger DG, Huston J 3rd, Riederer SJ. Improved venous suppression and spatial resolution with SENSE in elliptical centric 3D contrast-enhanced MR angiography. Magn Reson Med 2004;52:761. [PubMed: 15389954]
18. MacFall JR, Pelc NJ, Vavrek RM. Correction of spatially dependent phase shifts for partial Fourier imaging. Magn Reson Imaging 1988;6:143–155. [PubMed: 3374286]
19. Noll DC, Nishimura DG, Macovski A. Homodyne detection in magnetic resonance imaging. IEEE Trans Med Imaging 1991;10:154–163. [PubMed: 18222812]
20. Madhuranthakam, AJ.; Hu, HH.; Kruger, DG.; Barger, AV.; Riederer, SJ. Undersampled elliptical centric view-ordering for improved resolution in contrast-enhanced MRA. Proceedings of the 12th Annual Meeting of ISMRM; Kyoto, Japan. 2004; p. 8
21. Madhuranthakam AJ, Hu HH, Barger AV, Haider CR, Kruger DG, Glockner JF, Huston J III, Riederer SJ. Undersampled elliptical centric view-order for improved spatial resolution in contrast-enhanced MR aniography. Magn Reson Med 2006;55:50–58. [PubMed: 16315207]
22. Weiger M, Pruessmann KP, Kassner A, Roditi G, Lawton T, Reid A, Boesiger P. Contrast-enhanced 3D MRA using SENSE. J Magn Reson Imaging 2000;12:671–677. [PubMed: 11050636]
23. Weiger M, Pruessmann KP, Boesiger P. 2D-SENSE for faster 3D MRI. MAGMA 2002;14:10–19. [PubMed: 11796248]
24. Block, WF.; Peters, DC.; Vigen, KK. Homodyne reconstruction for projection reconstruction trajectories. Proceedings of the 7th Annual Meeting of ISMRM; Philadelphia. 1999; p. 659
25. King, KF.; Angelos, L. SENSE and partial Fourier homodyne reconstruction. Proceedings of the 8th Annual Meeting of ISMRM; Denver. 2000; p. 153
26. Angelos, L.; King, KF.; Estkowski, L. Scan time impact on reducing slab wrap in slice encoding SENSE. Proceedings of the 11th Annual Meeting of ISMRM; Toronto, Canada. 2003; p. 2336
27. Riederer SJ, Tasciyan T, Farzaneh F, Lee JN, Wright RC, Herfkens RJ. MR fluoroscopy: technical feasibility. Magn Reson Med 1988;8:1–15. [PubMed: 3173063]
28. Korosec FR, Frayne R, Grist TM, Mistretta CA. Time-resolved contrast-enhanced 3D MR angiography. Magn Reson Med 1996;36:345–351. [PubMed: 8875403]

29. Madhuranthakam AJ, Kruger DG, Riederer SJ, Glockner JF, Hu HH. Time-resolved 3D contrast-enhanced MRA of an extended FOV using continuous table motion. Magn Reson Med 2004;51:568–576. [PubMed: 15004799]

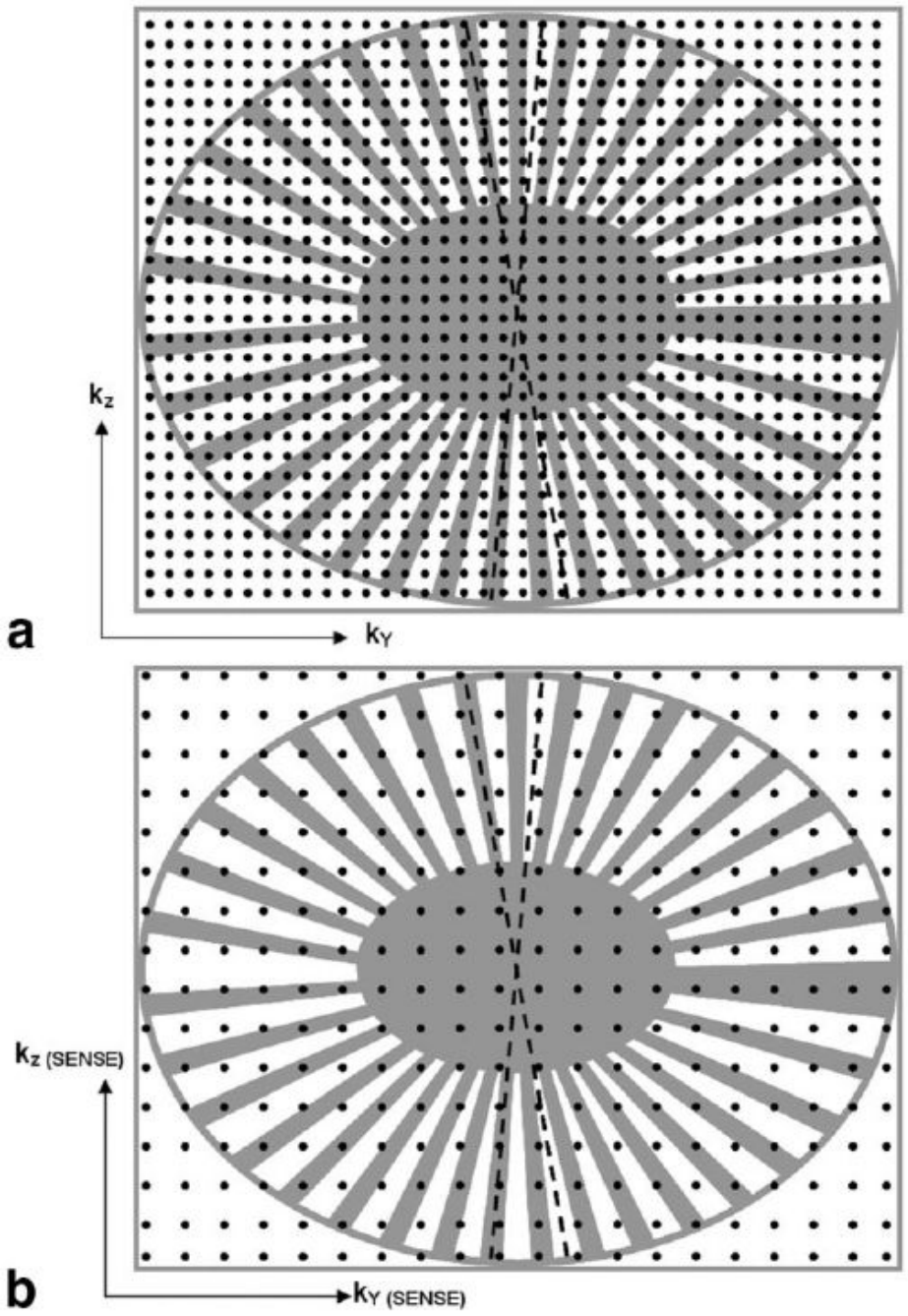

FIG. 1.

a: Cartesian k_Y-k_Z representation of the hybrid EC-PF sampling scheme, modified from a standard EC 3DFT acquisition. A fully sampled k_Y-k_Z plane is shown, with each black dot representing a phase-encoded view. A reduced number of views are shown for illustration clarity. Only views that fall within the *k*-space footprint (gray areas) are acquired in the EC-PF technique, which includes a fully-sampled central region and an undersampled outer annlus. PR-like radial sectors are asymmetrically sampled to facilitate 2D homodyne reconstruction. **b**: Extension to 2D-SENSE. Note the SENSE-encoded k_Y-k_Z axis labels and increased sampling intervals.

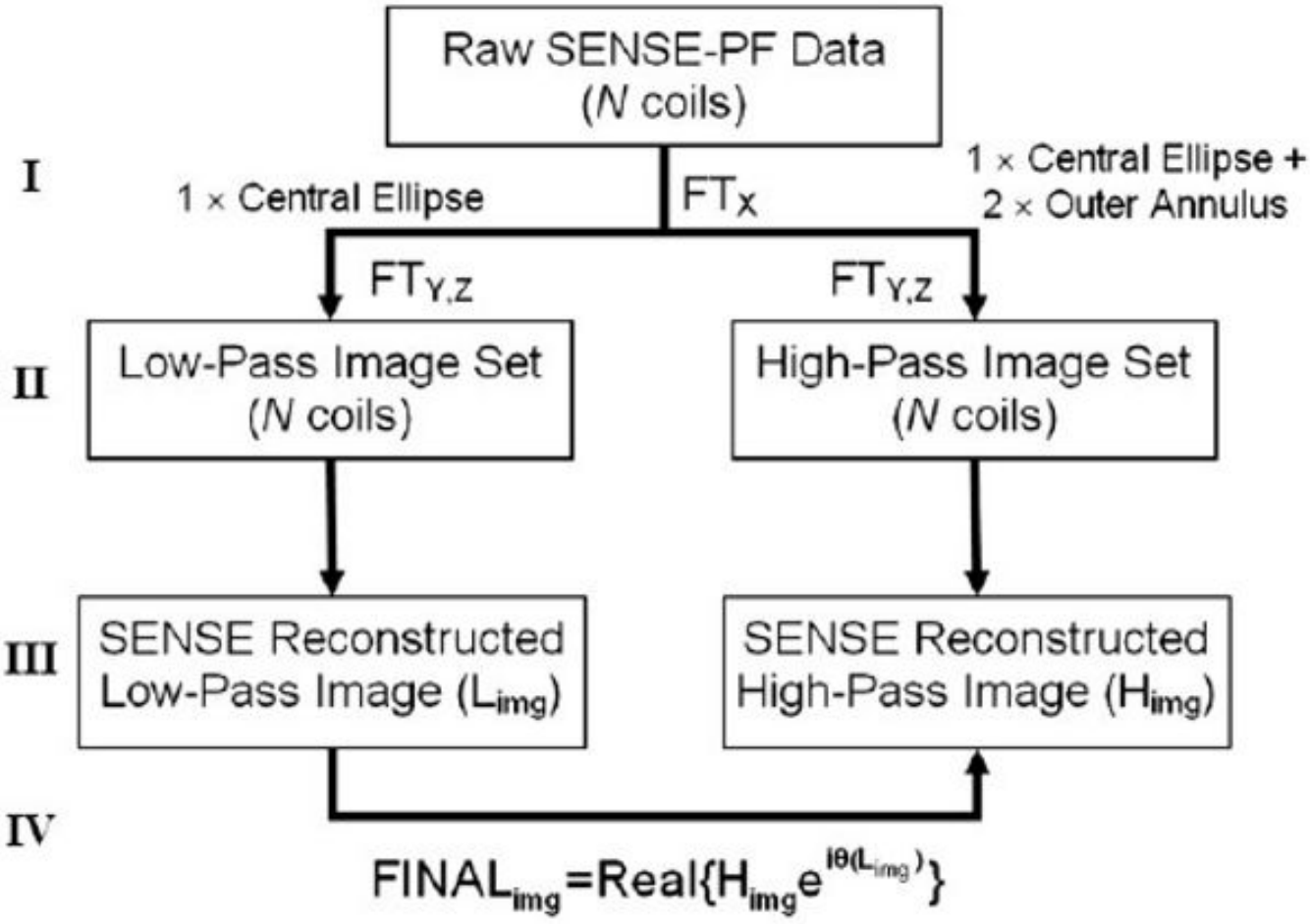

FIG. 2.

Reconstruction algorithm for 2D-SENSE-PF data. Step I: Raw data from *N* coils are first Fourier transformed along the frequency-encoding axis. Step II: For each coil, data are separated and Fourier transformed along the phase-encoding axes into low- and high-pass images. See text for details. Step III: A separate SENSE reconstruction is performed on the *N* low-pass and *N* high-pass aliased image sets, yielding one of each, deterministically unfolded using L_{img} and H_{img} results. Step IV: Homodyne phase correction using L_{img} and H_{img}.

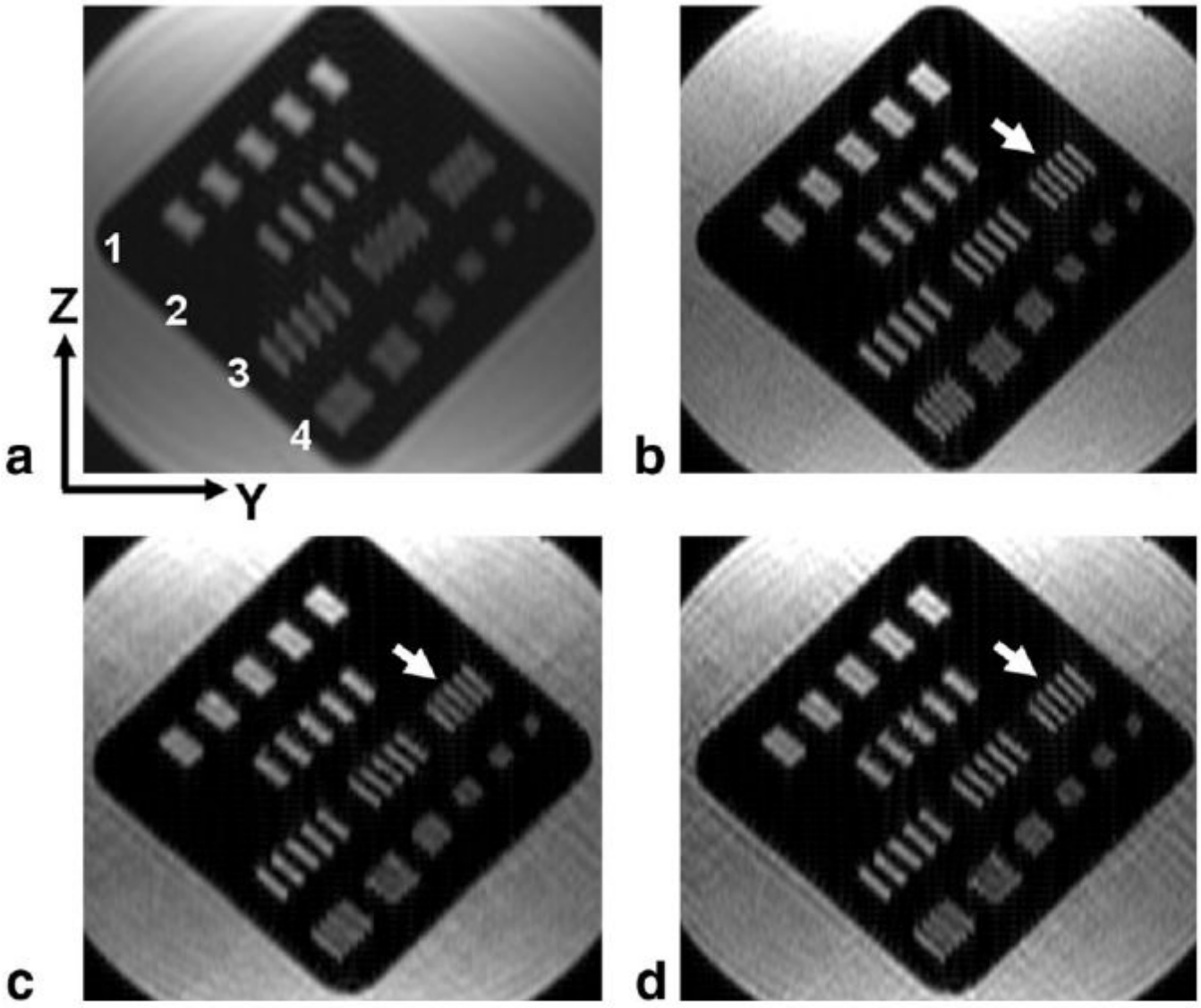

FIG. 3.

Results from the phantom study, showing axial reformats in the *Y-Z* plane of coronally acquired images. **a**: Reference nonaccelerated, fully sampled case. **b**: Fourfold SENSE reconstructed image with clear resolution improvement, shown by bars in row 3. **c**: Sparse (zero-filled) reconstruction of a SENSE-PF acquisition, acquired in 58% of the scan time as in **b**, showing a small loss in resolution (arrow) due to zero-filling. **d**: Homodyne reconstruction of SENSE-PF acquired data, demonstrating resolution (arrow) comparable to that in **b**.

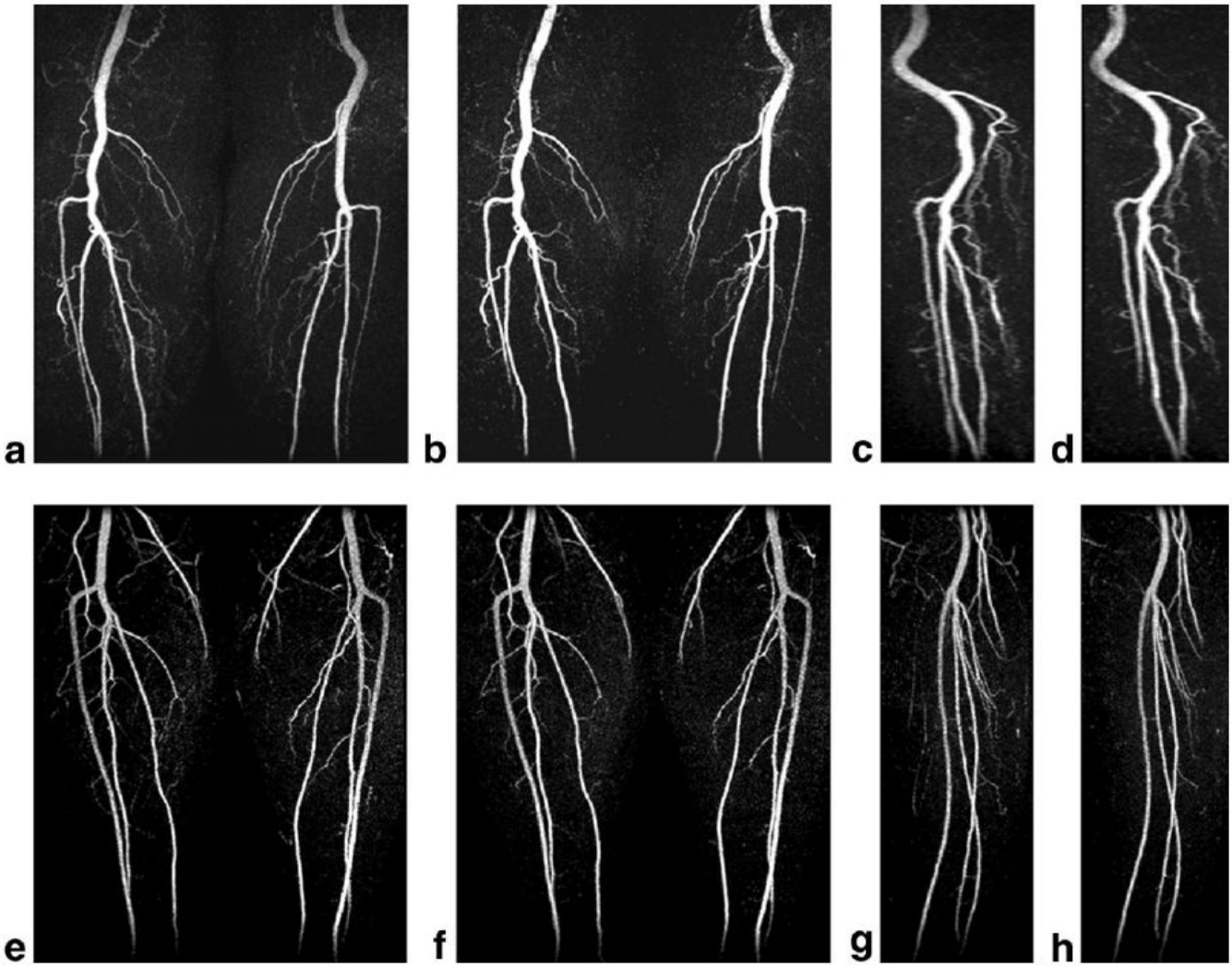

FIG. 4.

Results from in vivo CE-MRA examinations of two healthy volunteers. **a**: Coronal projection of a 34-s fourfold SENSE-only acquisition. **b**: A 19-s sevenfold SENSE-PF acquisition of the same volunteer. **c** and **d**: Sagittal projection images from SENSE and SENSE-PF acquisitions, respectively. **e–h**: Similar image sets of another volunteer. Note the comparable vessel visualization, spatial resolution, and lack of venous enhancement and reconstruction artifacts in all images.

Table 1

Evaluation of CE-MRA Volunteers

Volunteer no.	First injection	Image quality		Secondary vessels	
		2D-SENSE	SENSE-PF	2D-SENSE	SENSE-PF
2	2D-SENSE	4	3	1	1
3	SENSE-PF	4	4	2	2
5	SENSE-PF	3	4	2	2
6	2D-SENSE	4	3	2	1
7	SENSE-PF	4	4	2	2
8	2D-SENSE	4	4	2	2
9	SENSE-PF	4	4	2	2
10	2D-SENSE	4	3	2	1
11	SENSE-PF	4	4	2	2
12	2D-SENSE	4	3	2	1
14	2D-SENSE	4	3	1	1